Pore Formation Induced by an Antimicrobial Peptide: Electrostatic Effects

Frantz Jean-François,* Juan Elezgaray,* Pascal Berson,† Pierre Vacher,† and Erick J. Dufourc*
*UMR 5248, Centre National de la Recherche Scientifique-Université Bordeaux 1, European Institute of Chemistry and Biology, Pessac, France; and †Institut National de la Santé et de la Recherche Médicale EMI 347, Université Victor Segalen and Institut Bergonié, Bordeaux, France

ABSTRACT We investigate the mode of action of Cateslytin, an antimicrobial peptide, on zwitterionic biomembranes by performing numerical simulations and electrophysiological measurements on membrane vesicles. Using this natural β-sheet antimicrobial peptide secreted during stress as a model we show that a single peptide is able to form a stable membrane pore of 1 nm diameter of 0.25 nS conductance found both from calculation and electrical measurements. The resulting structure does not resemble the barrel-stave or carpet models earlier predicted, but is very close to that found in the simulation of α-helical peptides. Based on the simulation of a mutated peptide and the effects of small external electric fields, we conclude that electrostatic forces play a crucial role in the process of pore formation.

INTRODUCTION

The increasing resistance of bacteria to conventional antibiotics makes the development of new modes of treatment essential. Over the past few years, antimicrobial peptides (AMPs) were presented as a potential solution: whereas classical antibiotics act specifically on biosynthetic pathways, AMPs may directly destabilize the lipid membrane (1) and constitute a promising alternative strategy for fighting the actions of microorganisms. AMPs were first identified in the hemolymph of insects and in the secretion of immune cells (2) and are key components of the innate response of multicellular organisms (2–4). Insects are indeed the only organisms that produce such peptides as part of a systemic response induced by microorganisms. For mammalians, these peptides are part of the adaptive immune system that constitutes a first host defense line by controlling natural flora (5). Most of the antimicrobial peptides are composed of L-amino acids, with well-defined α-helix or β-sheet secondary structures or a mixture of both. In most cases, the mode of action appears to be the direct lysis of the pathogenic cell membrane (1). Some AMPs are not cell-selective; they act on both bacterial and mammalian cells. Others are selective either to mammalian cells but not to bacteria, or vice versa.

Three modes of action have been proposed for α-helical peptides:

The Barrel-Stave model (1), in which bundles of amphipathic helices oligomerize and form transmembrane pores with the hydrophilic residues facing the lumen of the pore. Here, the minimal inhibitory concentration required to dissipate the transmembrane potential should be far below the μM concentration, a fact only observed for a few peptides, such as alamethicin, pardaxin, and the α-helix of δ-endotoxin.

Alternatively, in the Carpet model (1), AMPs act in a detergentlike manner, covering the cell surface until a threshold concentration is reached that leads to the formation of membrane patches in which the lipids form toroidal aggregates stabilized by the amphipathic peptides (6,7). Dramatic membrane disruption thus occurs, leading to cell death (8).

To fit existing experimental data, Huang et al. (9) presented an energetic model based upon the assumption of membrane stress-driven pore formation and concluded that: 1), peptides bound to the bilayer create an internal tension similar to that required for lipid vesicle lysis (10); and 2), migration of peptides toward the rim of the pore contributes to its stabilization. A typical pore radius of 1–2 nm was estimated (6–12 peptides/pore).

More recently, Leontadiou et al. (11) suggested a completely different scenario, the Disordered Toroidal Pore model (DTP), where a single peptide is able to insert into the membrane and form a stable pore. Their numerical simulations show that, contrarily to what was expected from the previously mentioned models, the pore is stabilized by a diffuse distribution of peptides, localized near the rim of the pore and mostly parallel to the membrane.

The work in Leontadiou et al. (11) raises many questions that are yet to be clarified. Two main mechanisms have been advocated in the past to be at the origin of the pore formation. Upon binding to the membrane, peptides increase slightly the area per lipid of the membrane. This induces a compressive stress on the monolayer in contact with the peptides. The stress is expansive on the opposite monolayer. Leontadiou et al. observed that the application of an external stress does not enhance the appearance of the pore and concluded that the relevant parameter is the difference in mechanical stress between the two faces of the membrane. Because most AMPs are charged, these peptides also induce an electric field that is, on average, normal to the membrane. Therefore, in addition to the existence of mechanical stress, the binding of AMPs may induce pore formation through an electroporation

Submitted May 7, 2008, and accepted for publication August 20, 2008.

Address reprint requests to Erick J. Dufourc, Tel.: 33-5-40-00-22-18; E-mail: e.dufourc@iecb.u-bordeaux.fr.

Editor: Peter Tieleman.

0006-3495/08/12/5748/09 $2.00

doi: 10.1529/biophysj.108.136655

mechanism. This possibility has been mentioned in other works (11–15).

The goal of this work is to further investigate the pore formation mechanism: instead of an α-helical peptide (MG-H2, a member of the magainin family) in interaction with a DPPC membrane, as in Leontadiou et al. (11), we will focus on a β-sheet peptide (Cateslytin) in interaction with a noncharged, zwitterionic membrane (1,2-dimyristoyl-*sn*-glycero-3-phosphocholine). Cateslytin (^{344}RSMRLSFRARGYGFR^{358}) is a 15-residue cationic sequence resulting from the enzymatic degradation of Chromogranin A that is secreted during stress. With a global net charge of +5 (Arg residues) and five hydrophobic residues, this β-sheet AMP has been shown to display antimicrobial activity in the μM range and to have no detectable hemolytic activity at concentrations below 100 μM (16). We report both on numerical simulations and electrophysiological measurements on vesicles (patch-clamp technique) that give additional support to the DTP model: a single peptide is able to form a stable pore that is characterized by a well-defined conductance: 0.25 nS from the patch-clamp experiments, 0.21 nS from the numerical simulations. We also provide NMR-derived measurements showing that the peptides perturb minimally the structure of the bilayer. In the following, we also bring additional evidence in favor of the hypothesis that the electroporation-like mechanism is crucial in the pore formation process.

MATERIALS AND METHODS

Chemicals

The lipids, 1,2-dimyristoyl-*sn*-glycero-3-phosphocholine (DMPC) and 1,2-dimyristoyl-$^{2}H_{54}$-*sn*-glycero-3-phosphocholine (DMPC-$^{2}H_{54}$), were purchased from Avanti Polar Lipids (Alabaster, AL). Bovine Cateslytin (bCGA^{344358}, RSMRLSFRARGYGFR) has been synthesized in our laboratory using Fmoc strategy and purified (99% purity) by reverse phase high-performance liquid chromatography (17).

Sample preparation

To prepare multilamellar vesicles (MLVs), the phospholipid powder was hydrated with a Tris KCl buffer (50 mM Tris, 100 mM KCl, pH 7.4) at a hydration (mass water/total mass), h, of 99% for patch-clamp experiments (4 mM) and 93% for solid-state nuclear magnetic resonance (NMR). After shaking with a vortex mixer, the samples were subjected to three freeze-thaw cycles. This operation was repeated three times. Different lipid/peptide molar ratios (R_i) were used for NMR experiments: 15, 50, 100, and 150, only the ratio 15 was used for patch-clamp. To mimic the action of the antimicrobial peptide, the peptide was added externally to the MLV preparation.

NMR spectroscopy

Solid-state NMR experiments were carried out on Bruker Avance DSX 300 WB and DPX 400 NB spectrometers (Wissembourg, France). ^{31}P-NMR spectra were acquired at 161.9 MHz using a phase-cycled Hahn-echo pulse sequence with gated broad-band proton decoupling. Deuterium NMR experiments on deuterated lipids were performed at 46.1 MHz by means of a quadrupolar echo pulse sequence. Typical acquisition parameters were as follows: spectral window of 50 kHz for ^{31}P-NMR and 250 kHz for ^{2}H-NMR; $\pi/2$ pulse widths ranged from 3 to 5 μs depending on sample, interpulse delays were of 30–40 μs. A recycle delay of 5 s was used for ^{31}P-NMR; for ^{2}H-NMR experiments, it was set to 2 s. Typically, 2–4 K scans were recorded for the deuterium nucleus and 1 K transients for the phosphorus nucleus. A line broadening of 50–100 Hz was applied prior to Fourier transformation. Phosphorus chemical shifts were referenced relative to 85% of H_3PO_4 (0 ppm). Quadrature detection was used in all cases. Samples were allowed to equilibrate at least 30 min at a given temperature (ranging from 10°C to 50°C) before the NMR signal was acquired; the temperature was regulated to $\pm$1°C.

Patch-clamp

Patch-clamp experiments were performed at room temperature (~23°C) according to Hamill and McBride (18). Liposomes were viewed under phase contrast with an inverted microscope (Nikon, Tokyo, Japan). Grounding was achieved through a chloride-coated silver wire inserted into an agar bridge (4% agar in electrode solution). Borosilicate glass pipettes (15–20 MΩ tip resistance; GC 100 F-10, Clark Medical Instruments, Pangbourne, UK) were manufactured and fire-polished by a microprocessor-driven DMZ puller (Zeitz, Augsburg, Germany). They were positioned using micromanipulators (Narishige International, London, UK). The currents were recorded in voltage-clamp mode, in mitochondria-attached configuration, by a RK 400 amplifier (Bio-Logic, Claix, France). Stimulus control, data acquisition, and processing were carried out on a PC computer equipped with a Labmaster TL-1 interface and loaded with the PClamp 5.5.1 software (interface and software from Axon Instruments, Foster City, CA). Electrode offset was balanced before forming a giga-seal. Signals were filtered at 1 kHz with a Bessel filter and sampled at 4 kHz. Steady-state currents were looked for by stepping (10 mV-increments) the membrane potential from +80 mV to −100 mV. Current-to-voltage relationships were established and conductance measured. We obtained single-channel activities in >50% of recordings. The polarities of potentials reported here refer to those of the patch pipette relative to that of the ground electrode, which was placed in the external medium. The offset potentials between both electrodes were zeroed immediately before seal formation. Junction potentials were zeroed with the electrode in the standard bath solution. The buffer solution (50 mM Tris and 100 mM KCl, pH 7.4) was symmetrical, i.e., the same outside and inside the selected membrane vesicle.

Numerical procedures

We have performed molecular dynamics (MD) simulations with atomic resolution on a DMPC bilayer in the presence of eight Cateslytin molecules. Counterions (Cl^-) were added to balance the net charge (+5) of each peptide. All the simulations were done using the GROMACS suite (19). The coordinates of the initial condition for Cateslytin were taken from the PDB structure 1LV4 corresponding to the NMR structure (20) of Catestatin, from which we removed six residues. It is noteworthy that this structure has been obtained in dimethyl-sulfoxide and is not expected to be preserved in solution or in contact with the bilayer. The net charge is +5. Chloride ions were added so that the system was globally neutral. No additional salt was present in the system. We added 6457 water molecules (simple point charge) to ensure the hydration of the membrane. The van der Waals interactions were cut off at 1.4 nm. The particle-mesh Ewald method was used to handle electrostatic interactions. Simulations were performed in the NPT ensemble (320 K, 1 bar), with a Berendsen thermostat (barostat). The coupling time constant was 0.1 ps for temperature and 5 ps for pressure. Furthermore, the pressure coupling was anisotropic (independent couplings for the normal and parallel directions to the bilayer plane). Only hydrogen-containing bonds were constrained using the LINCS algorithm. The force field was a combination between the OPLS-based united-atom force field of Berger (21) and the GROMACS (ffgmx) force field for peptides.

System setup

The initial coordinates of the DMPC bilayer (128 lipids) were taken from the Tieleman website (http://moose.bio.ucalgary.ca, file dmpc_npat.pdb). Chloride ions were added at random by replacing water molecules. Eight peptides were placed at least 2 nm from the bilayer. We ran five independent simulations (T1–T5), of 200 ns each. In addition, we also considered the effect of an external electric field, directed along the normal of the bilayer and of varying magnitude (see Table 1). The initial condition of these E-trajectories was the same as the final configuration of simulation T1. Finally, we also considered the evolution of a new peptide obtained from the mutation Arg → Glu. This mutation was performed on the end conformation of trajectory T2.

Energy model

The energy model we consider relies on continuum theories (elastic and electrostatic) and contains two contributions. The purely elastic part is that given in Huang et al. (9),

$$E_{\text{elas}} = c_1 R - c_2 R^2 + c_3 R^3, \tag{1}$$

where R is the radius of the pore, and c_1, c_2, and c_3 are constants related, respectively, to the surface tension of the bilayer, line tension of the pore, and line density of the peptides at the rim of the pore. In addition to the approximations specific to the model, it should be mentioned that the asymmetric tension induced by the binding of the peptides to only one of the monolayers is not taken into account explicitly in this theory. The values (9) of the constants c_i are

$$c_1 = 2\pi\gamma, \quad c_2 = \pi\sigma_0, \quad c_3 = \frac{4}{3}\pi^2\sigma_0\frac{N_P}{P}\Gamma_L, \tag{2}$$

where $\gamma = 10 \times 10^{-12}$ N is the line tension, $\sigma_0 \sim 10$ mN/m is the effective membrane tension, Γ_L is the line density of peptides at the rims, and $N_P/P = 1/8$ the number of pores per peptide bound.

The electrostatic contribution has been computed in the framework of models of electroporation (22,23). The key assumptions are that the shape of the pore is toroidal, and in the applicability of the macroscopic Maxwell equations to the system. In particular, it is assumed that the dielectric properties of the two media (bilayer and conducting solvent) are homogeneous and change abruptly from one media to the other. The expression we use here is an analytical approximation of the numerically computed mechanical work to create a conducting pore in an otherwise dielectric body,

$$E_{\text{elec}} = \int_0^R drV_m^2 \frac{F_{\max}}{1 + \frac{r_h}{r + r_t}}, \tag{3}$$

where $V_m \sim 0.4$ V is the potential drop across the membrane, $F_{\max} = 0.7 \times 10^{-9}\, NV^{-2}$ is the maximum electric force for $V_m = 1$ V, $r_h = 0.97$ nm, and $r_t = 0.31$ nm. We refer the reader to the literature (22,23) for a detailed derivation of Eq. 3.

TABLE 1

Name	Simulation time	Pore formation time	External electric field (V/nm)
T1	200 ns	No	0
T2	200 ns	15 ns	0
T3	200 ns	20 ns	0
T4	200 ns	No	0
T5	200 ns	80 ns	0
E1	50 ns	2 ns	0.2
E2	50 ns	5 ns	0.1
E3	50 ns	9 ns	0.08
E4	50 ns	20 ns	0.05

RESULTS AND DISCUSSION

Molecular dynamics simulations

To mimic the experimental conditions (peptides initially located outside the cell), the initial conditions were chosen so that the distance between the peptides and the outer leaflet of the bilayer was <2 nm (Fig. 1 *A*). The initial peptide-membrane association is quite fast (a few nanoseconds, Fig. 1 *B*), as already observed in similar systems (24–26). This leads the system to a metastable situation, where both the area per lipid increases slightly due to the penetration of the peptide into the bilayer and, because of the asymmetric charge distribution, an electric field (~0.1 V/nm) roughly perpendic-

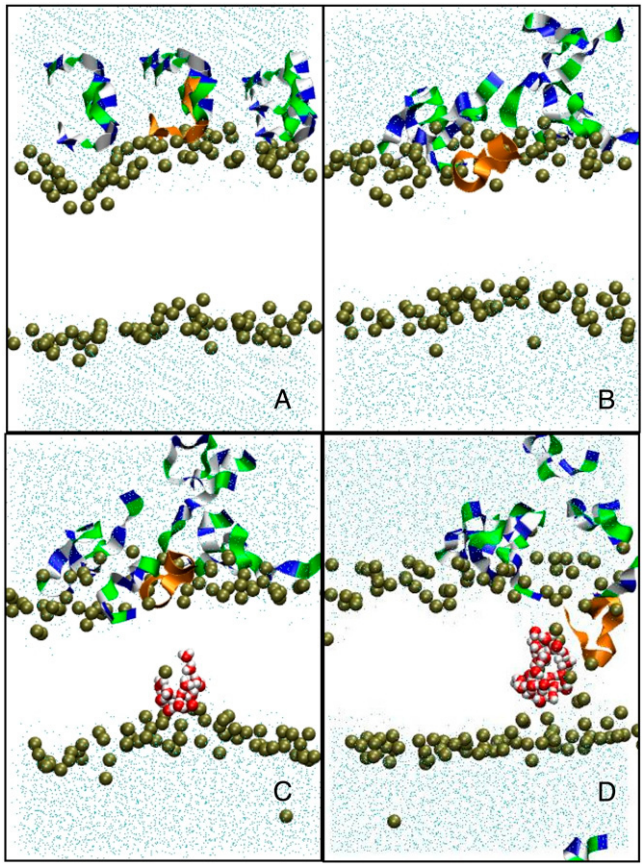

FIGURE 1 Molecular dynamics of pore formation induced in a DMPC bilayer (128 lipids, 6754 water molecules) by the presence of eight Cateslytins. (*A*) Starting conditions with the initial distribution of the peptides above the outer membrane leaflet; (*B*) the equilibrated bilayer at 5 ns; and (*C*) the formation of a transient water defect at 10 ns. (*D*) Formation of a stable pore at 12 ns. The bilayer is only represented by the position of the interfacial phosphate groups (*brown beads*). Outside water molecules are in cyan, water molecules in the pore are in red, and CPK models are in white. The peptides that do not contribute to the pore are represented as ribbons (residues: *dark blue*, basic; *green*, polar; and *white*, nonpolar). Peptide that inserts into the pore is in orange.

ular to the average plane of the bilayer appears. This situation is reminiscent of that found in electroporation experiments, although here the electric field inside the membrane is mostly due to the peptides. As other simulations (12,27,28) have already shown, under such circumstances the pore formation starts with the creation of a single water defect (Fig. 1 *C*). However, in contrast with the pure electroporation conditions, the water defect initiates only from the inner side of the bilayer and nucleates around the phosphate group of one of the DMPC lipids. The lifetime of these defects is, in general, of ~1 ns. Whether one of these defects leads to the formation of a pore is a rather stochastic process and seems to be dependent on the presence, in the vicinity of its tip, of a peptide inserted deeply enough in the outer side of the bilayer. Out of the five simulations with no external electric field, only three trajectories lead to a pore formation: T2, T3, and T5 (see Table 1). Both T1 and T4 showed the existence of transients (strong deformation of the bilayer) that were similar to the preliminary steps of the pore formation in T2, T3, and T5, but none of these transients led to a distinct pore structure at the end of the 200 ns. Similarly, the sequence of events leading to the pore and its time of appearance are quite different for T2, T3, and T5. In the two events observed in T2 and T3, once a contact is established between a water finger and one of the peptides (10–20 ns after beginning the simulation), the pore of ~1 nm diameter is formed and remains stable for the rest of the simulation (Fig. 1 *D*). In T5, we observe the existence of an ~20-ns transient pore before the formation of the more stable final structure at 80 ns.

A similar sequence of events has been observed by Leontadiou et al. (11). In this work, the authors consider the interaction of an analog of magainin-2, a well-studied antimicrobial peptide (charge +3 at physiological pH) with a DPPC bilayer. Interestingly and despite the fact that many details (peptide length and charge, lipids) are different from our work, the final structure of the pore appears to be quite similar to ours.

The peptide inserted in the pore does not display a well-defined secondary structure (see Fig. 2). In T2 and T3, it is in a rather compact conformation of wedgelike shape, with either a Serine or an Arginine amino acid pointing toward the inner leaflet (in contrast, other peptides bound to the outer leaflet are in extended conformation). In the T5 simulation, at least two peptides participate in the deformation leading to the pore. Again, no clear secondary structure is detectable. It is noteworthy that in the T5 case, aggregation of the peptides is more pronounced than in the T2 and T3 cases, in agreement with the observation of Leontadiou et al. (11). The spatial distribution of the lipids around the lumen of the pore follows the toroidal distribution predicted by the carpet mechanism (1), as the tails of these lipids are mostly parallel to the average position of the bilayer plane. A similar behavior has also been observed in pores induced on bilayers under mechanical stress (28), in the presence of an electric field (27,28), or under a transmembrane charge imbalance (12).

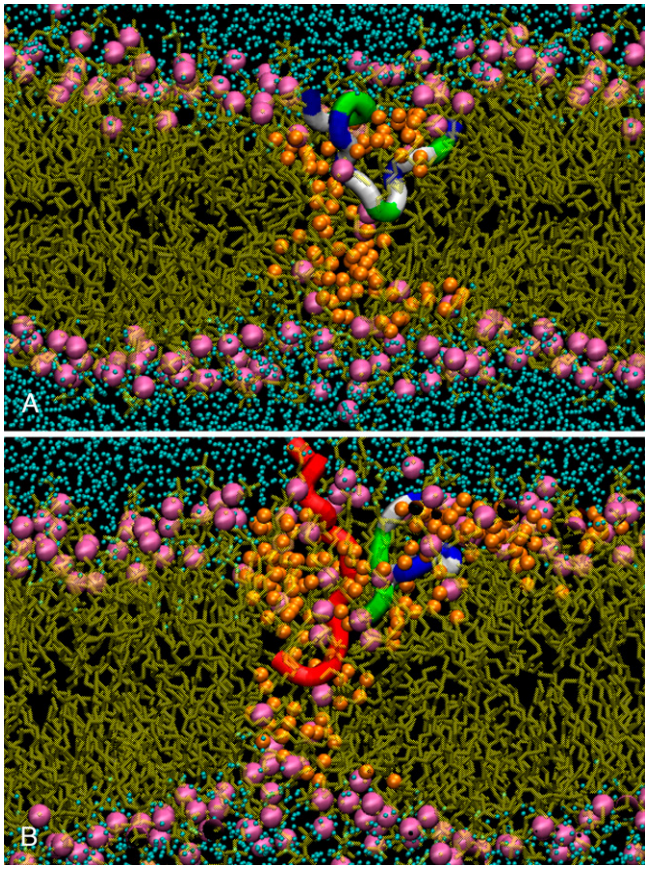

FIGURE 2 Side views of the pore formed in the T2 (*A*) and T5 (*B*) trajectories. The bilayer is represented by the position of the phosphate groups (*magenta beads*); fatty acyl chains are in light brown. Water molecules (*orange*) in the vicinity of the pore are also shown (other water molecules are in *cyan*). The peptides that participate in the pore are represented as ribbons (residues: *dark blue*, basic; *green*, polar; and *white*, nonpolar). In panel *B*, the second peptide is in red.

Fig. 2 shows different side views of the pore structure for the T2 and T5 trajectories. Only the peptides (one in T2, two in T5) that are involved in the pore structure are shown. In both cases, the peptides are inserted only half-way in the bilayer and do not span completely the hydrophobic core. Instead, a significant number of peptides are recruited to complete the hydrophilic border of the pore, with their heads pointing to the lumen.

Fig. 3 shows the evolution of the averaged normal component $E_z(z)$ of the electric field upon binding of peptides. These profiles are obtained by integrating the Poisson equation along the normal to the membrane, with the hypothesis that the charge distribution is invariant in this plane. With no peptides (continuous curve), $E_z(z)$ shows a typical profile with two symmetric regions where the electric gradient is significant. These correspond to the bilayer-water interface and can be correlated both to the presence of dipoles in the lipid headgroups and the orientation of water molecules at this interface. The addition of peptides has two effects: it decreases the electric gradients on the peptide side and creates

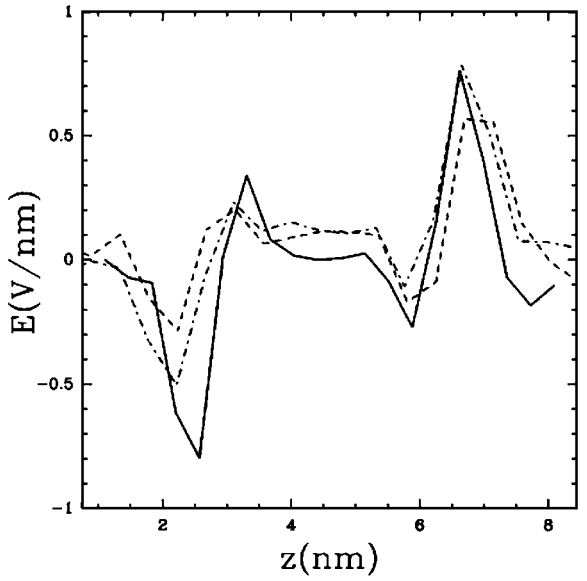

FIGURE 3 Normal component of the averaged electric field as a function of z (the bilayer is in the x-y plane). The peptides (if any) are located in the $z < 4$ region. The different data correspond, respectively, to: (*continuous*) no peptides bound; (*dashed*) initial condition of the T2 trajectory; and (*dot-dashed*) $t = 12$ ns (pore formation). The corresponding electric field have been obtained from time averages over 2 ns.

a roughly constant electric field (~0.1 V/nm) in the hydrophobic interior of the bilayer, increasing slightly the electric gradient in the peptide-free leaflet. This explains why water defects are formed preferentially from this side. Note that in the presence of a pore, the system is not strictly invariant in the plane of the membrane. In this particular case, the $E_z(z)$ curve gives only an estimate of the electric field in the region of the pore.

To check the sensitivity of the pore formation mechanism against electrostatic factors, we considered the addition of an external electric field oriented parallel to the normal of the bilayer and directed so that the penetration of the peptides into the hydrophobic core is favored. (See (29) for a discussion on the role of external electric fields in the insertion of alamethicin in an octane-water interface.) In all of the E-trajectories (with the exception of E5, see Table 1), a pore formed in a time relatively short compared to the trajectories with ($E_z = 0$). However, as $E_z \rightarrow 0$, the time for pore formation increases considerably (the measurement of a law relating the time for pore formation and the strength of the external electric field would require a significant increase of the statistics and has not been considered in this article). The strength of the applied electric fields are comparable to the one induced by the peptides itself, and appears to be lower than the electroporation threshold (0.4 V/nm, according to (30), 0.29 V/nm in (12)). The addition of the external and the peptide-induced electric field is, in turn, comparable to these values or even lower (trajectories E3 and E4). This could point to the existence of regions where the electric field is higher, a phenomenon that could be favored by the aggregation of peptides (31).

To further test the influence of electrostatic factors on the pore formation, we considered the effect of the mutation ARG → GLN on each of the five arginines. This mutation was applied simultaneously to all the peptides in the system. The effect of this mutation is negligible on the amphipathic properties of the peptides, but starting from an initial condition with a pore already formed (final configuration of the T2 trajectory) it induces (in ~4 ns) the disruption of the pore structure. The two leaflets of the bilayer recover their integrity and all the peptides remain bound at the membrane surface for the rest of the trajectory (100 ns). Furthermore, the electric field inside the hydrophobic core of the bilayer drops to zero. Although it cannot be considered as a definitive proof, this simulation again shows that electrostatic factors are crucial for the formation of the pore structures, even when charged AMPs interact with zwitterionic lipids.

To compare the molecular dynamics simulations with the patch-clamp experiments, current measurements were performed by the addition of an external electric field equal to the experimental holding potential (HP) divided by the width of the bilayer. The pore structure is that obtained at the end of T2. In the time accessible to the simulation, only the counterions are susceptible to be significantly driven by the electric field. In a trajectory of 190 ns with $HP = 40$ mV, we find 10 permeation events, corresponding to 8.5 ± 3 pA (0.21 ± 0.07 nS, assuming the Ohm law), in nice agreement with the measurements presented below (the statistical error was obtained by splitting in two the trajectory and computing the current for each short trajectory. Note, however, that the experimental current measurements show the existence of an intermediate state with a conductivity roughly divided by two, with respect to that of the open state. So far, the MD simulations do not provide with any evidence of the existence of this intermediate state.

Experimental results: solid-state NMR and patch-clamp

We have also performed several experimental measurements on DMPC liposomes in contact with a solution of Cateslytin. Fig. 3 shows the ^{31}P-NMR spectra in the absence and presence ($R_i = 15$) of Cateslytin. The axially symmetric lineshape characteristic of nonoriented multilamellar vesicles is seen on the left. After addition of Cateslytin and sample equilibration, the spectrum on the right is obtained. The same lineshape is obtained, demonstrating that there has been no membrane disruption; only the low frequency modes of motion are altered. A sharp isotropic line centered at 0 ppm would have been otherwise detected as reported, for instance, in the case of the bee venom AMP Melittin (6–8). Temperature was varied in the range 10–50°C by 5°C steps and similar spectra were obtained. Solid-state ^{2}H-NMR experiments were also performed using perdeuterated DMPC and confirmed

^{31}P-NMR data: powder patterns characteristic of intact MLV were obtained in the presence of added Cateslytin (31). Again, temperature variation led to similar lineshapes. One may nonetheless notice that spectra are broader in the presence of the AMP, indicating that Cateslytin interacts with the lipid membrane and slows down molecular motions in the nanosecond-to-millisecond range.

Using the electrophysiological setup of patch-clamp experiments, membrane vesicles that are trapped by the micropipette (Fig. 4) are not destroyed or experience change in shape when a solution of Cateslytin is present in the outside medium and in contact with the outer membrane layer. The current-voltage measurements of patch-clamp experiments give strong support to the existence of stable pores of lifetime of ~1 s (Fig. 5). The observation of single channel events (0.25 nS, 10 pA amplitude) leads to a diameter of 1 nm. This channel activity results in a voltage-dependent current (Fig. 6), which activates slowly (>1 min) at depolarized potentials (+20 to +80 mV), whereas it inactivates with the same kinetics at polarized potentials (−40 to −100 mV). This corresponds nicely with the size and conductivity found by MD calculations. It is noteworthy that the patch-clamp technique gives a macroscopic measurement on a timescale of seconds. MD simulations provide an atomic description on a much shorter timescale and may picture early events of more complex lipid-AMP structures (final pore made by several peptides, aggregation of pores, etc.) that lead to electric measurements. Such timescales are, at present, beyond the reach of simulations.

Energetics: the continuum model approach

To further understand the process of pore formation, it is of interest to compare the results of the simulations with existing models of the system. A representative example of the family of purely elastic models is that of Dufourc et al. (8). In this model, the energy of a pore of radius R, in the presence of peptides, is of the form $E = aR + bR^2 + cR^3$, where the three positive constants a, b, and c are related, respectively, to the surface tension of the bilayer, line tension of the pore, and line density of the peptides at the rim of the pore. This energy yields a stable pore only for nonzero values of the constant c. The radius R of this pore is ~1 nm, in agreement with our simulations. However, the energy gap (Fig. 7) between the open and closed pore is very small (<3 kcal/mol), in disagreement with the experimental observation of stable pores with lifetime of ~1 s. A simple way to increase this gap is to take into account the electrostatic contribution corresponding to the work needed to create a region with high dielectric constant in an otherwise hydrophobic core (22,23). This calculation has been done in the context of electroporation using several approximations (22). Using the expression in Smith et al. (22), valid for a toroidal pore, the energy gap is increased roughly by 5 kcal/mol (Fig. 8). According to these figures, the pore structure is mostly stabilized by an electrostatic contribution, a fact that could explain the high charge borne by many antibiotic peptides (5).

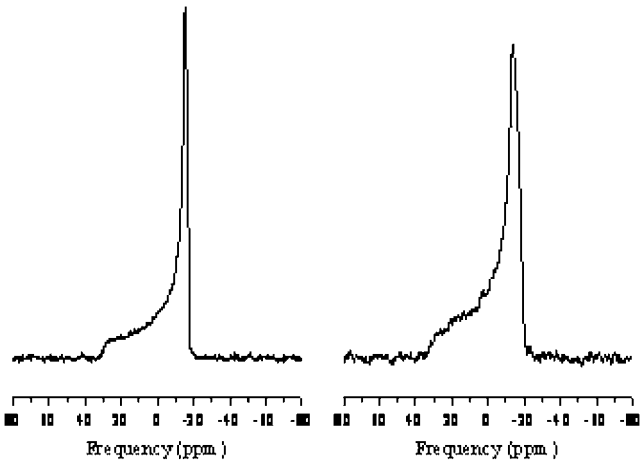

FIGURE 4 Solid-state ^{31}P-NMR proton-decoupled spectra of DMPC MLV in the absence (*left*) and the presence (*right*) of Cateslytin ($R_i = 10$, $T = 37°C$).

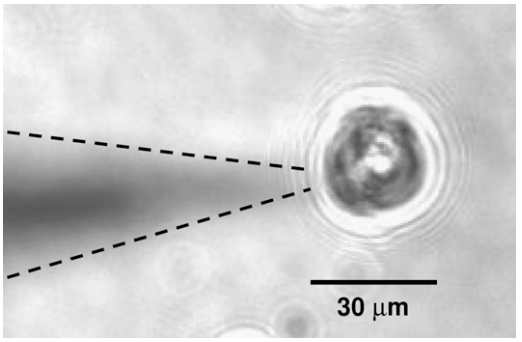

FIGURE 5 Microscope view of patch-clamp setup in the liposome-attached configuration. Magnification ×400. Because the pipette is not in the same focal plane as the liposome it appears blurred; dashed lines were added as a guide to the eyes.

DISCUSSION

The set of trajectories generated with MD simulations show that, within a lapse of time in the range of 10–100 ns,

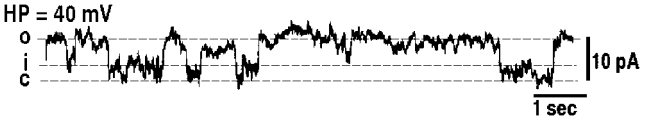

FIGURE 6 Unitary channel recording obtained in liposome-attached configuration of the patch-clamp technique. Shown is a representative current trace recorded at 40 mV (holding potential, *HP*) from a patch containing one active channel under symmetrical conditions (150 mM KCl inside and outside the liposome). The open, intermediate, and closed states of the channel are indicated with dotted lines and the letters O, I, and C, respectively.

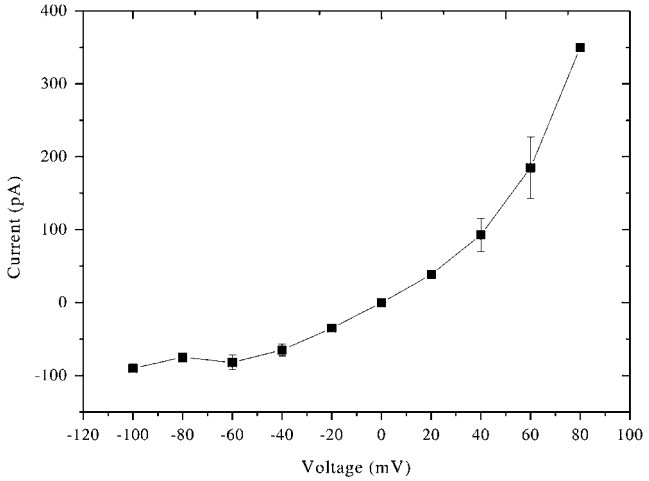

FIGURE 7 Macroscopic current-to-voltage relationship for Cateslytin-induced channels in the liposome-attached mode. Each point corresponds to the average of four different experiments.

Cateslytin in a concentration of $P/L = 1{:}16$ induces the formation of a pore structure, very similar to the DTP model (11). This concentration of peptides is similar to that used in the patch-clamp experiments. It is also comparable to the threshold concentration observed for similar peptides, such as magainin. An interesting fact observed in these MD simulations is the absence of a well-defined structure, both for the pore and the peptides bound to the bilayer. ATR measurements (31) indicate that Cateslytin in solution is not structured and becomes 50% highly aggregated β-sheets when bound to DMPC bilayers. The starting condition of all the MD trajectories was chosen to be that found from NMR experiments in an organic solvent. Ongoing simulations (not reported here) tend to show that peptides initially structured in β-sheet partially lose their secondary structure and still produce the same type of pore structures. Of course, due to the short duration of the MD trajectories, it is difficult to conclude anything about the formation or not of any secondary structure. Several authors (11,32) have pointed out the hypothesis that the structural properties of AMPs do not play a major role in the pore formation process. Our simulations, together with the results of Leontadiou et al. (11), show that the same type of pore seems to be formed in α- and β-folding peptides.

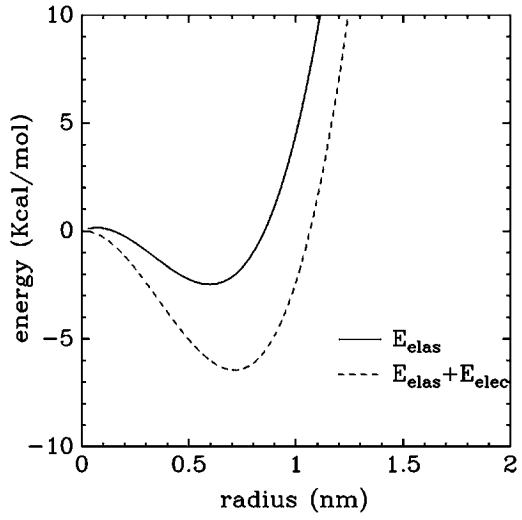

FIGURE 8 Energy to create a pore in an elastic and dielectric medium. (*Continuous line*) Elastic contribution. (*Dashed line*) Elastic and electrostatic contribution.

In agreement with Leontadiou et al. (11), we observe that the binding of peptides slightly (2%) increases the area per lipid. Several theoretical models (9,33) suggest that the induced stress explains the concentration dependence of the pore formation. However, these models rely on continuous elastic models, for which there is no possibility to take into account the asymmetric stress observed in the MD simulations. Leontadiou et al. performed MD simulations under stress and concluded that this dissymmetry is a key ingredient to explain the formation of the pore. For this reason, the continuous elastic model discussed in Energetics: The Continuum Model Approach (above) should be considered only as a useful guide to evaluate the elastic energy involved in this process. Our energy model shows that in a continuous description of the mechanical and electrostatic stresses, the electrostatic contribution is more than twice the purely elastic contribution. An additional argument against the purely mechanical scenario is provided by the data of Heerklotz and Seelig (34), which show that the difference of the area per lipid between the two leaflets should be such that $\Delta A^{\text{in-out}}/A_L \sim 0.15$ to trigger permeation. These conditions do not seem to be met in our case.

In the context of AMPs binding to a neutral bilayer, the presence of an electric field in the hydrophobic core of the bilayer is related to the charge imbalance created by the differences in the binding of peptides and their counterions to the phospholipids of the bilayer. Therefore, as a first approximation, the binding of AMPs creates an electric field that, on the average, is normal to the bilayer, as in electroporation experiments. The continuous theory for electroporation shows that the electrostatic contribution to the stability a pore can be roughly described by the energy to create a cylinder of high dielectric constant inside an otherwise hydrophobic region.

The similarity between the peptide-induced pore formation and electroporation has been suggested by previous studies, both numerical (12,13) and experimental (15). The results obtained with the E-trajectories show that the addition of an electric field E_z that is small, compared to the estimated threshold E_{th} for electroporation, triggers the formation of a pore in a systematic way. A straightforward interpretation is that the electric field induced by the peptides E_{ind} adds to the external field so that $E_{ind} + E_z > E_{th}$. However, for the lower values of E_z used in trajectories E4 and E5, this interpretation seems to fail and it is probably necessary to take into account

the inhomogeneous distribution of the electric field. Similar observations were made in the literature (15,35). For instance, in Binder and Lindblom (15), the authors consider the interaction of penetratin (a Trojan peptide, able to bring small DNA or proteins into cells) and conclude that electrostatic effects are dominant and explain binding and permeation. In Diederich et al. (35), the authors showed that adsorption of polylysine on a diphytanoylphosphatidylserine membrane decreases the critical breakdown threshold. Notice that these two studies consider negatively charged membranes but, as argued in Leontadiou et al. (11), charge-charge interactions between the peptide and anionic lipids are not directly involved in pore formation. Although not directly related to this work, we would like to mention the experiments and related simulations of Vernier and co-workers (36). This work shows that the externalization of phosphatidylserine after exposure of biological cells to short ($<$100 ns) high-field electric pulses can be explained by the formation of pores that locally deform the hydrophobic interior of the bilayer and through which a positively charged lipid is electrophoretically driven. From an electrostatic point of view, this system and our system are, in fact, very similar.

The more difficult point of this work is the comparison between the MD simulations and the experimental data. Only patch-clamp experiments yield a measurable quantity that could be addressed from simulations. We have shown that the electric current (number of counterions per unit time that go through the pore under a fixed external electric field) is comparable to the experimentally measured current, with no indication so far for the existence of any intermediate state (see Fig. 5). In addition to the difference in timescales, it should also be pointed out that experiments were carried out with salt. MD simulations did not consider this effect. However, several experimental results (37,38) show that lipid headgroup charge and ionic strength of the solution appear to have little effect on electroporation, whereas lipid tail and cholesterol do have a significant effect. In fact, electroporation simulations (30) suggest that the important contribution on an added electric field is the modification of the local field gradients at the lipid-water interface. These are only slightly modified in the presence of salt.

CONCLUSIONS

In contrast with previous existing theories, the picture revealed by MD clearly shows the key role played by charges borne by AMPs. The process of pore formation can be summarized in three steps:

1. AMPs binding to the outer leaflet of the bilayer. The binding speed is probably dependent on phospholipid head charge and could be faster for charged heads, such as those found in bacterial outer membranes.
2. The charge imbalance resulting from peptide binding locally destabilizes the bilayer, favoring the formation of water defects (the resulting average electric field strongly orients water molecules). Because hydrogen bonding in a hydrophobic environment is stronger than in water, once an initial defect is formed, the probability of growth is nonnegligible.
3. Water pore stabilization by the peptide constitutes the main stochastic ingredient: it requires the simultaneous presence of a water defect and a sufficiently-close peptide residue. A similar sequence of events has been observed by Leontadiou et al. (11). Interestingly and despite the fact that many details (peptide length, secondary structure and charge, lipids) are different from our work, the final structure of the pore appears to be quite similar to ours.

We have also shown that the structure obtained from the MD simulations is compatible with the patch-clamp experiments. However, this observation is not sufficient to discard the barrel-stave (toroidal) model (1), as a slower evolution toward a more organized structure by insertion of additional peptides into the pore cannot be excluded. It has also been indicated (5) that the toroidal pore is a transient state in the carpet mechanism, with the latter mechanism being found for higher P/L ratios. Experimental results (31) with the DMPC-Cateslytin system show that at P/L = 1:16, there is no membrane disruption. Further experimental work will be needed to investigate a possible transition to the carpet mechanism.

As suggested by previous simulations on pure lipid bilayers (12,27), the formation of water pores as a consequence of a charge imbalance could be a generic mechanism. We have shown that Cateslytin (and probably similar AMP peptides) is able to both provide the necessary charge gradient and stabilize the subsequent pore structure. It would be interesting to check whether similar arguments could clarify the role of ionic imbalance on DNA translocation (27).

Part of the simulations was performed on the IDRIS (Orsay, France) facilities. The Aquitaine Region is also thanked for equipment support. One of the authors benefited from enriching discussions with F. Argoul (École Normale Supérieure de Lyon).

This work has been supported by the Région Aquitaine and through computer time allocation on the Pôle M3PEC, Université Bordeaux 1.

REFERENCES

1. Shai, Y. 1999. Mechanism of the binding, insertion and destabilization of phospholipid bilayer membranes by α-helical antimicrobial and cell nonselective membrane lytic peptides. *Biochim. Biophys. Acta*. 55: 1462–1466.
2. Hoffmann, J. A., J. M. Reichhart, and C. Hertru. 1996. Innate immunity in higher insects. *Curr. Opin. Immunol*. 8:8–13.
3. Ganz, T., and R. I. Lehrer. 1998. Antimicrobial peptides of vertebrates. *Curr. Opin. Immunol*. 10:41–44.
4. Lehrer, R. I., and T. Ganz. 1999. Antimicrobial peptides in mammalians and insect host defense. *Curr. Opin. Immunol*. 11:23–27.
5. Zasloff, M. 2002. Antimicrobial peptides of multicellular organisms. *Nature*. 415:389–395.
6. Dufourc, E. J., J. F. Faucon, G. Fourche, J. Dufourcq, T. Gulik-Krzywicki, and M. Lemaire. 1986. Reversible disk-to-vesicle transition

of melittin-DPPC complexes triggered by the phospholipid acyl chain melting. *FEBS Lett.* 201:205–209.

7. Pott, T., and E. J. Dufourc. 1995. Action of melittin on the DPPC-cholesterol liquid-ordered phase: a solid-state H^2NMR and P^{31}NMR study. *Biophys. J.* 68:965–977.
8. Dufourc, E. J., J. M. Bonmatin, and J. Dufourcq. 1989. Membrane, structure and dynamics by H^2NMR and P^{31}NMR. Effects of amphipathic peptidic toxins on phospholipid and biological membranes. *Biochimie.* 71:117–123.
9. Huang, H. W., F. Chen, and M. Lee. 2004. Molecular mechanism of peptide induced pores in membranes. *Phys. Rev. Lett.* 92:198304-1–198304-4.
10. Olbrich, K., W. Rawicz, D. Needham, and E. Evans. 2000. Water permeability and mechanical strength of polyunsaturated lipid bilayers. *Biophys. J.* 79:321–327.
11. Leontadiou, H., A. E. Mark, and S.-J. Marrink. 2006. Antimicrobial peptides in action. *J. Am. Chem. Soc.* 128:12156–12161.
12. Gurtovenko, A. A., and I. Vattulainen. 2005. Pore formation coupled to ion transport through lipid membranes as induced by transmembrane ionic charge imbalance: atomistic molecular dynamics study. *J. Am. Chem. Soc.* 127:17570–17571.
13. Miteva, M., M. Andersson, A. Karshikoff, and G. Ottig. 1999. Molecular electroporation: a unifying concept for the description of membrane pore formation by antibacterial peptides, exemplified with NK-lysin. *FEBS Lett.* 462:155–158.
14. Zhang, H., and S. O. Smith. 2005. Mechanism of penetration of ANTP(43–58) into membrane bilayers. *Biochemistry.* 44:10110–10118.
15. Binder, H., and G. Lindblom. 2003. Charge-dependent translocation of the Trojan peptides penetratin across lipid membranes. *Biophys. J.* 85:982–995.
16. Briolat, J., S. S. Wu, S. K. Mahata, B. Gonthier, D. Bagnard, S. Chasserot-Golaz, K. B. Helle, D. Aunis, and M. H. Metz-Boutigue. 2005. New antimicrobial activity for the catecholamine release-inhibitory peptide from chromogranin A. *Cell. Mol. Life Sci.* 62:377–385.
17. Jean-François, F., L. Khemtemourian, B. Odaert, S. Castano, A. Grelard, C. Manigand, K. Bathany, M. H. Metz-Boutigue, and E. J. Dufourc. 2007. Variability in secondary structure of the antimicrobial peptide Cateslytin in powder, solution, DPC micelles and at the air-water interface. *Eur. Biophys. J.* 36:1019–1027.
18. Hamill, O. P., and D. W. McBride. 1995. Pressure/patch-clamp methods. *In* Neuromethods: Patch-Clamp Applications and Protocols. Vol. 26. A. Boulton, G. Baker, and W. Walz, editors. Humana Press, Totowa, NJ.
19. Lindahl, E., B. Hess, and D. van der Spoel. 2001. GROMACS 3.0: a package for molecular simulation and trajectory analysis. *J. Mol. Model.* 7:306–317.
20. Preece, N. E., M. Nguyen, M. Mahata, S. K. Mahata, N. R. Mahapatra, I. Tsigelny, and D. T. O'Connor. 2004. Conformational preferences and activities of peptides from the catecholamine release-inhibitory (Catestatin) region of chromogranin A. *Regul. Pept.* 118:75–87.
21. Berger, O., O. Edholm, and F. Jahnig. 1997. Molecular dynamics simulations of a fluid bilayer of dipalmitoylphosphatidylcholine at full hydration, constant pressure, and constant temperature. *Biophys. J.* 72:2002–2013.
22. Smith, K. C., J. C. Neu, and W. Krassowska. 2004. Model of creation and evolution of stable electropores for DNA delivery. *Biophys. J.* 86:2813–2826.
23. Neu, J. C., K. C. Smith, and W. Krassowska. 2003. Electrical energy required to form large conducting pores. *Bioelectrochemistry.* 60:107–114.
24. Lensink, M. F., B. Christiaens, J. Vandekerckhove, A. Prochiantz, and M. Rosseneau. 2005. Penetratin-membrane association: W48/R52/W56 shield the peptide from the aqueous phase. *Biophys. J.* 88:939–952.
25. Shepherd, C. M., H. J. Vogel, and D. P. Tieleman. 2003. Interactions of the designed antimicrobial peptide MB21 and truncated dermaseptin S3 with lipid bilayers: molecular-dynamics simulations. *Biochem. J.* 370:233–243.
26. Aliste, M. P., J. L. MacCallum, and D. P. Tieleman. 2003. Molecular dynamics simulations of pentapeptides at interfaces: salt bridge and cation-π interactions. *Biochemistry.* 42:8976–8987.
27. Tarek, M. 2005. Membrane electroporation: a molecular dynamics simulation. *Biophys. J.* 88:4045–4053.
28. Tieleman, D. P., H. Leontadiou, A. E. Mark, and S. J. Marrink. 2003. Simulation of pore formation in lipid bilayers by mechanical stress and electric fields. *J. Am. Chem. Soc.* 125:6382–6383.
29. Tieleman, D. P., H. J. C. Berendsen, and M. S. P. Sansom. 2001. Voltage-dependent insertion of alamethicin at phospholipid/water and octane/water interfaces. *Biophys. J.* 80:331–346.
30. Tieleman, D. P. 2004. The molecular basis of electroporation. *BMC Biochem.* DOI:10.1186/1471-2091-5-10.
31. Jean-François, F., S. Castano, B. Desbat, B. Odaert, M. Roux, M. H. Metz-Boutigue, and E. J. Dufourc. 2008. Aggregation of Cateslytin β-sheets on negatively charged lipids promotes rigid membrane domains. *Biochemistry.* 47:6394–6402.
32. Shai, Y. 2002. Mode of action of membrane active antimicrobial peptides. *Biopolymers.* 66:236–248.
33. Zemel, A., A. Ben-Shaul, and S. May. 2005. *Eur. Biophys. J.* 34:230–242.
34. Heerklotz, H., and J. Seelig. 2001. Detergent-like action of the antibiotic peptide surfactin on lipid membranes. *Biophys. J.* 81:1547–1554.
35. Diederich, D., G. Bähr, and M. Winterhalter. 1998. Influence of polylysine on the rupture of negatively charged membranes. *Langmuir.* 14:4597–4605.
36. Vernier, P. T., M. J. Ziegler, Y. Sun, W. V. Chang, M. A. Gundersen, and D. P. Tieleman. 2006. Nanopore formation and phosphatidylserine externalization in a phospholipid bilayer at high transmembrane potential. *J. Am. Chem. Soc.* 128:6288–6289.
37. Koronkiewicz, S., and S. Kalinowski. 2004. Influence of cholesterol on electroporation of bilayer lipid membranes: chronopotentiometric studies. *Biochim. Biophys. Acta.* 1661:196–203.
38. Genco, I., A. Gliozzi, A. Relini, M. Robello, and E. Scalas. 1993. Electroporation in symmetrical and asymmetric membranes. *Biochim. Biophys. Acta.* 1149:10–18.